Supplementary Information

Scaling Effect on Unipolar and Bipolar Resistive Switching of Metal Oxides

Takeshi Yanagida[1,2], Kazuki Nagashima[1], Keisuke Oka[1], Masaki Kanai[1], Annop Klamchuen[1], Bae Ho Park[3] and Tomoji Kawai[1,3]

[1] Institute of Scientific and Industrial Research, Osaka University, 8-1 Mihogaoka, Ibaraki, Osaka 567-0047, Japan

[2] PRESTO, Japan Science and Technology Agency, 4-1-8 Honcho, Kawaguchi, Saitama 332-0012, Japan

[3] Department of Physics, Division of Quantum Phases and Devices, Konkuk University, Seoul 143-701, Republic of Korea

S1. Construction and structures of Pt/oxide/Pt resistive switching devices

Pt/oxide/Pt sandwich structures for resistive switching were constructed as crossbar junctions. The crossbar junctions were formed on n-type Si substrate capped with a 300 nm SiO_2. First, the bottom Pt electrode with the thickness of 50 nm was deposited by RF sputtering (SANYU Electron SC-701HMC). The conditions for RF sputtering are 50 W and 1 Pa. The deposition rate was 10 nm/min. The width of electrode lines was defined by electron-beam lithography technique (JEOL JSM-7001F with Nano printer SPG-724) with the resist (Zeon, ZEP 5200). The width was ranged from 50 nm to 100 μm. After the bottom electrode formation, oxide layers (CoO_x, NiO_x and TiO_2) with the thickness of 50-200 nm were deposited on the bottom electrodes by utilizing pulsed laser deposition (PLD) technique. The depositions of oxide layers were performed under room temperature (RT) with varying the oxygen partial pressure. (0.1 Pa for CoO_x, 10^{-3} Pa for NiO (1), 10^{-1} Pa for NiO (2), 1 Pa for TiO_2). The laser energy, the repetition rate, and the distance between the substrate and the target were set to be 40 mJ, 10 Hz, and 30 mm, respectively. ArF excimer laser (Lamda-Physik COMPex 102, λ =193 nm) was utilized for the laser ablation. The deposition rate was 0.5 nm/min. Then the top Pt electrode lines of 50 nm thickness were deposited by RF sputtering (50 W and 1 Pa). The top electrode lines were positioned as cross lines to the bottom electrode lines. The width of top electrode lines was also controlled and defined by EB lithography technique. The deposition rate was 10 nm/min. The cell area was defined by the width of Pt electrodes, ranging from 10^4-10^{10} nm^2. For smallest cells below 10^3 nm^2, junctions using oxide nanowires were used, and the details of nanowire devices can be seen in elsewhere.[1-6] Figure S1 shows the cross-sectional HRTEM image of Pt/oxide/Pt sandwich structures. As shown in Figure S1, the fabricated oxide layers were

consistently polycrystalline forms. This is because the oxide film formations were performed at relatively low temperature (RT) and also on Pt electrodes without lattice matching. Also we have fabricated a single crystalline oxide layer by utilizing conductive oxide substrate (Nb 1wt%-$SrTiO_3$). The single crystalline feature can be seen in Figure S2 of XRD.

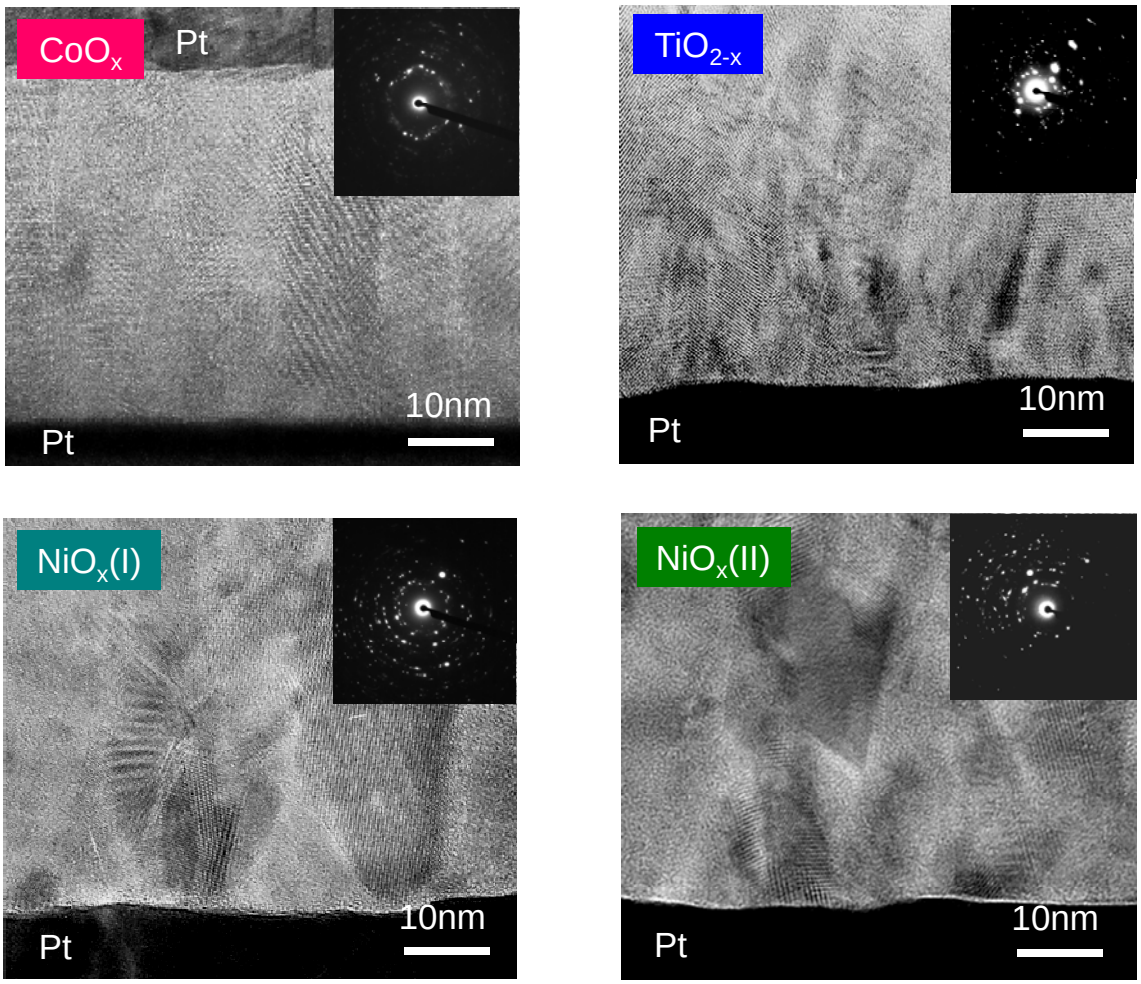

Figure S1 Cross-sectional TEM images of fabricated sandwich structures.

(Pt/CoO_x/Pt, Pt/TiO_{2-x}/Pt, Pt/NiO_x(1)/Pt, Pt/NiO_x(2)/Pt)

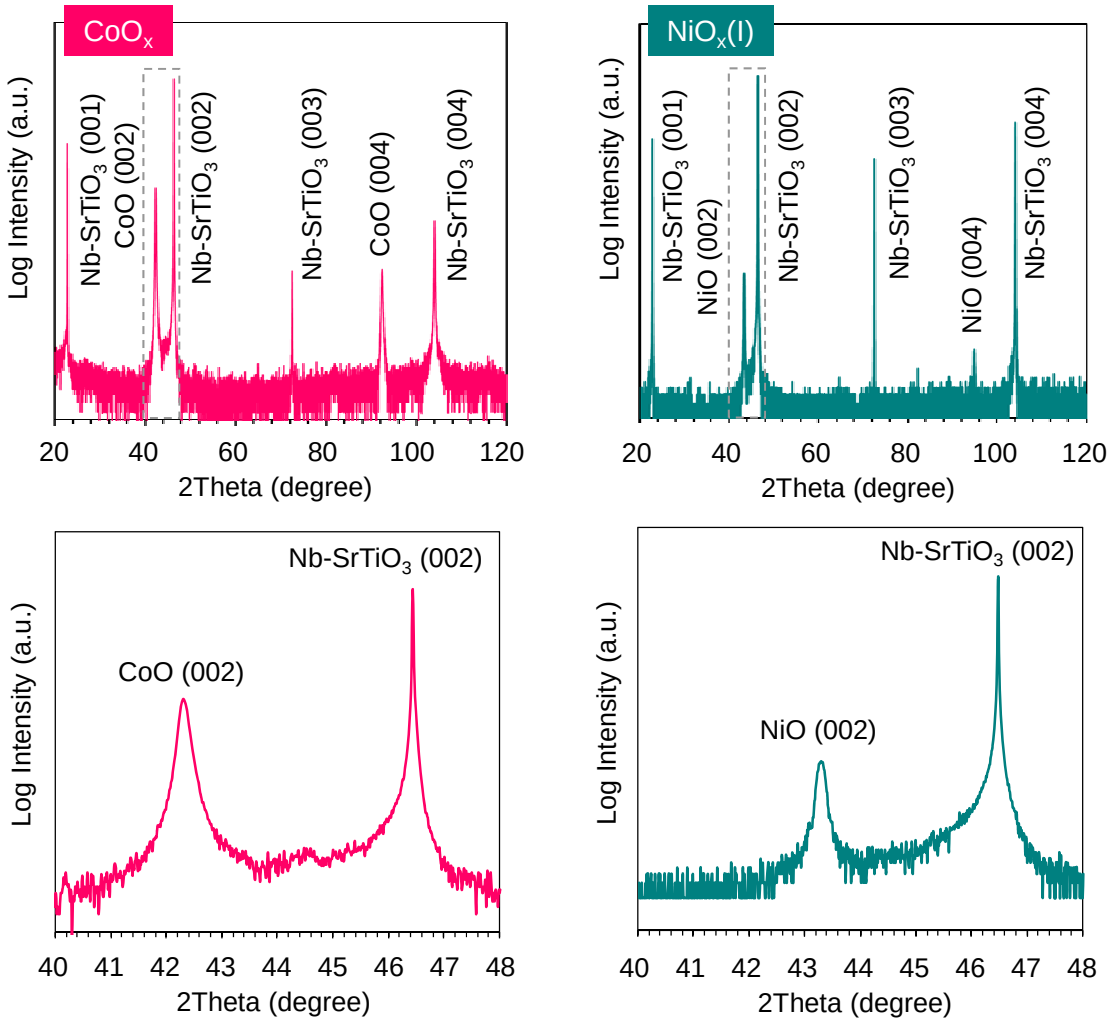

Figure S2 XRD data of epitaxial films (CoO_x and NiO_x) on Nb-$SrTiO_3$ substrate. Upper figures show the long range scan data for 20-120 theta degree, and the lower figures show the short range scan data for 40-48 theta degree around (002) peak.

S2. Switching properties of fabricated resistive switching devices (CoO_x, TiO_{2-x}, and NiO_x)

Figure S3 shows the variation of I-V data for fabricated resistive switching devices including TiO_2 and NiO_x when varying the cell areas and the operation currents. The transport measurements were performed by using a semiconductor parameter analyser (Keithley 4200SCS) at RT in ambient atmospheres. It can be seen that the variation as to the polarity characteristics of resistive switching is rather common for various resistive switching materials. Figure S4 shows the retention data of both ON state and OFF state for bipolar switching and unipolar switching in the cases of CoO_x and TiO_{2-x} junctions. All retention data showed the non-volatility of resistive switching over 10^4 sec, although the slight decrease was found in the case of bipolar switching in CoO_x. Previously we have reported that such relatively short retention time for bipolar switching is closely related to the effect of surroundings.[5] Figure S5 shows the endurance data of bipolar switching and unipolar switching in the case of TiO_{2-x} junctions. The endurance of bipolar switching was confirmed at least over 250 times, and also previously we have reported that the endurance of the bipolar switching in CoO_x was over 10^8. [3] Figure S6 shows the effect of sweep rate on the bipolar switching behaviours in the case of TiO_{2-x} junctions. The sweep rate did not affect the bipolar switching behaviors within the range of this study. Thus these data as to the switching properties demonstrated that the observed resistive switching behaviors are highly non-volatile and reliable.

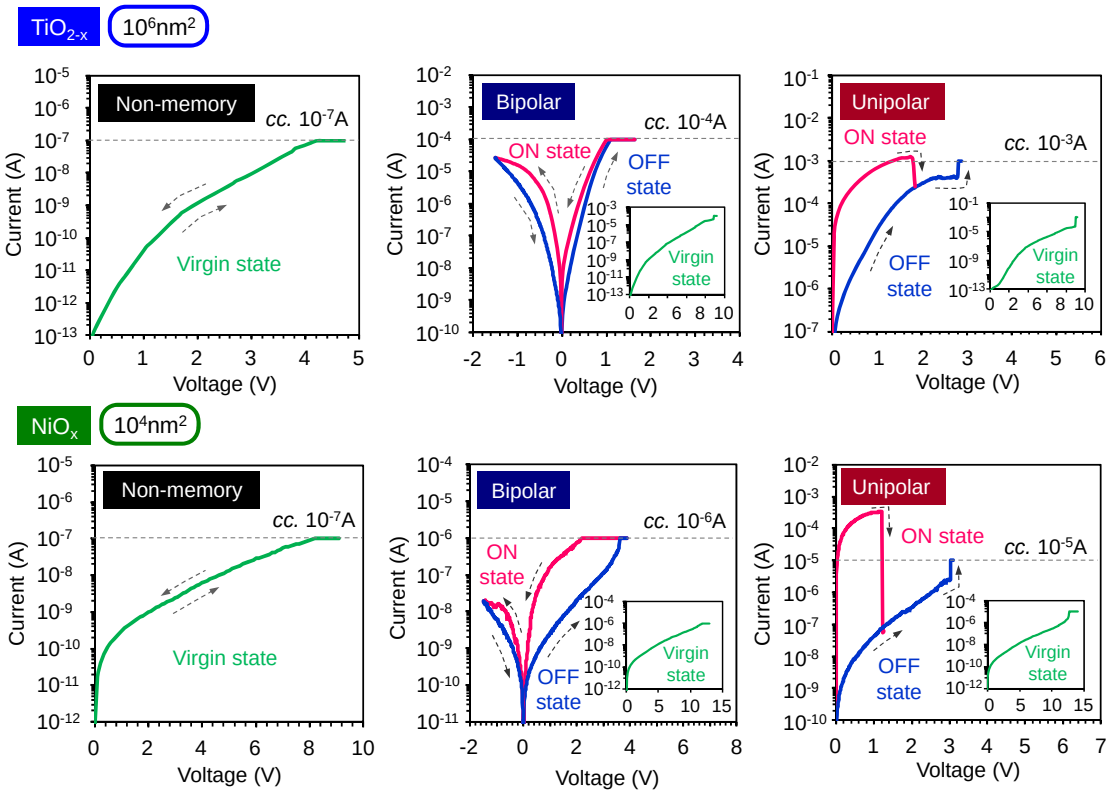

Figure S3 Typical I-V data of resistive switching devices of TiO_{2-x} and NiO_x when varying the forming current and the cell areas. Data showed the variation of non-memory, bipolar, and unipolar switching behaviors.

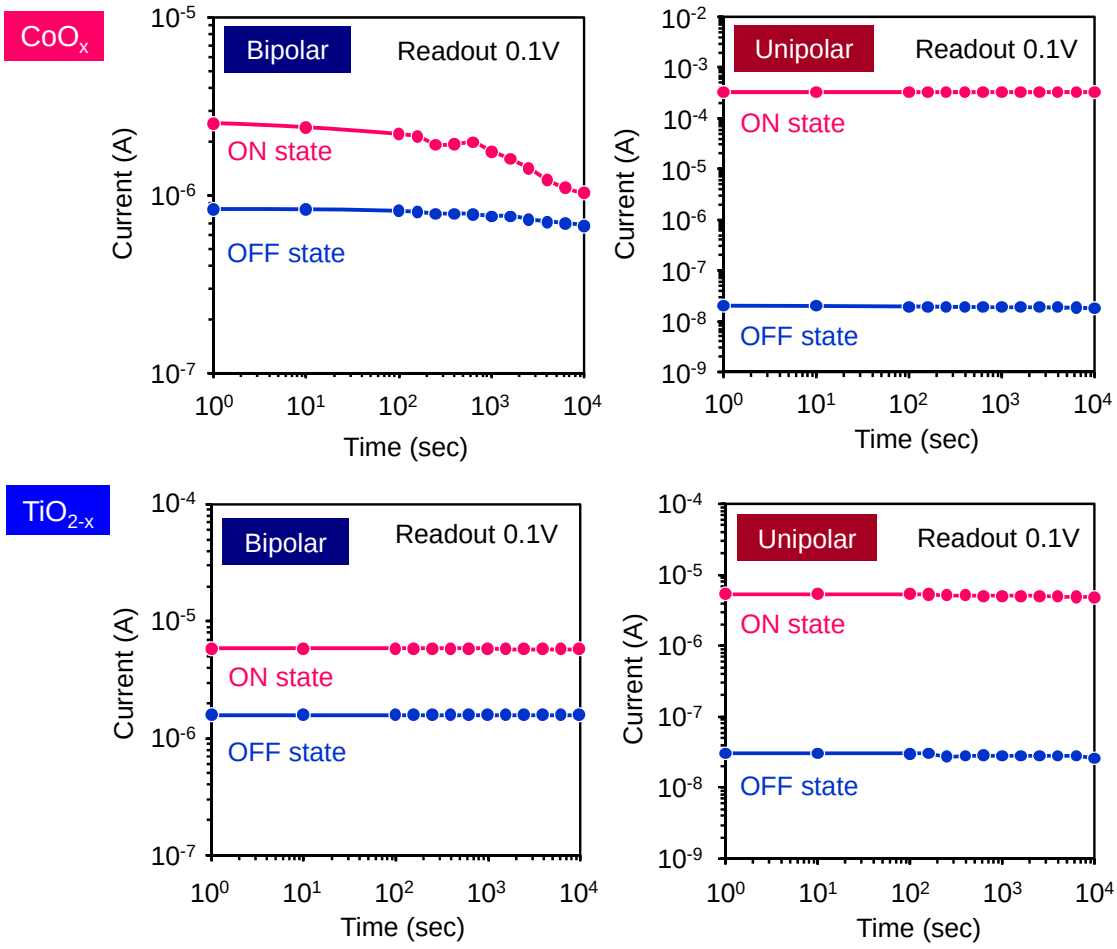

Figure S4 Retention data of bipolar switching and unipolar switching behaviors in the cases of CoO_x and TiO_{2-x} junctions.

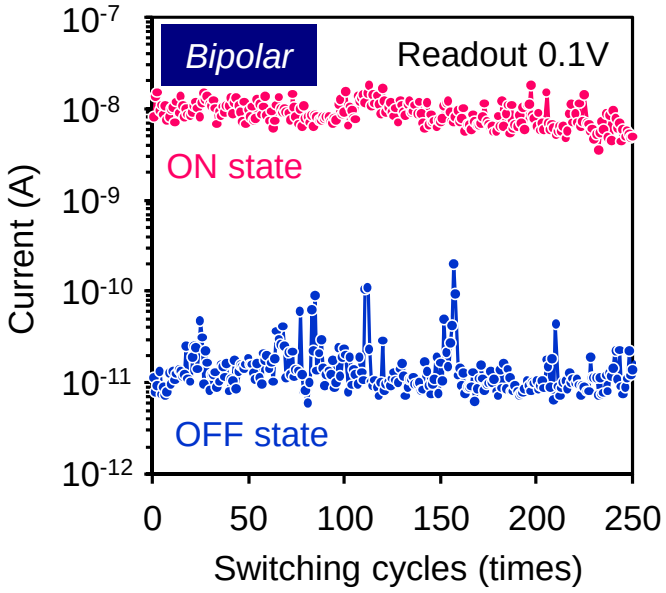

Figure S5 Endurance data of bipolar switching in the case of TiO_{2-x} junctions.

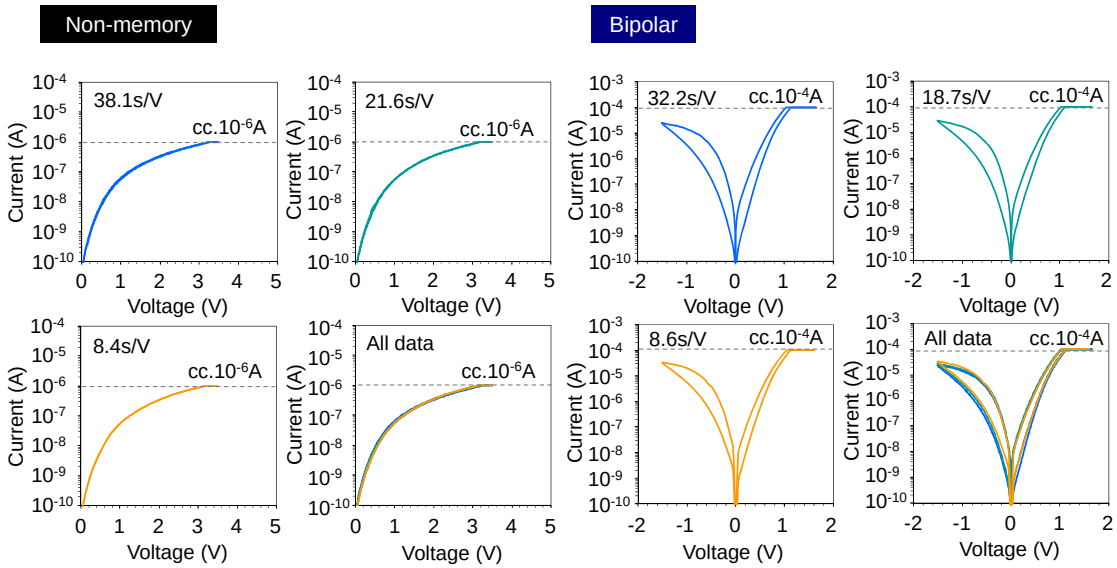

Figure S6 Effect of sweep rate on bipolar switching behaviors and non-memory behaviors in the case of TiO_{2-x} junctions.

S3. Spatial distribution of electric field in cross bar junctions.

Figure S7a shows the calculated data of spatial electric field distribution. Two devices with different aspect ratios of switching layer between electrodes are examined to study the effect of aspect ratio on the spatial electric field distribution data. The simulated devices are comprised of a SiO_2 bottom layer of 300nm thickness, TiO_2 switching layer of 50nm thickness, a bottom electrode of 50nm thickness and a top electrode of 50nm thickness. The device geometry is almost consistent with the real device geometry employed. Commercial finite element method package (μ-series) was utilized to simulate the spatial electric field distributions. As can be seen in Figure S7, the electric field at the edge is enhanced due to a well-known metal edge effect. However, such edge-enhanced electric field is strongly relaxed with the distance from the edge. More quantitatively, the ratio of the spatial electric field to an area-averaged electric field is shown in Figure S7b. It can be clearly seen that the most enhanced electric field near the edge is just about 2.5 times of an area-averaged electric field value. In addition, the spatial area of such edge-enhanced electric fields is rather limited. For example, at the position away from 5nm from the edge, the electric fields are much closer to an uniform electric field distribution. Thus these simulation data highlights that the effect of aspect ratio on the spatial electric field distribution is rather limited, and does not cause a significant discrepancy with an area-averaged electric field distribution data within our experimental range of aspect ratios. In addition, we have measured the resistance values of pristine samples when varying the aspect ratio, as shown in Figure S8. The junction resistance well scales with the area of cross point rather than the edge length. Thus within our experimental range, an approximation as to an uniform electric field at the cross point seems to be appropriate from these experimental and simulation data.

(a)

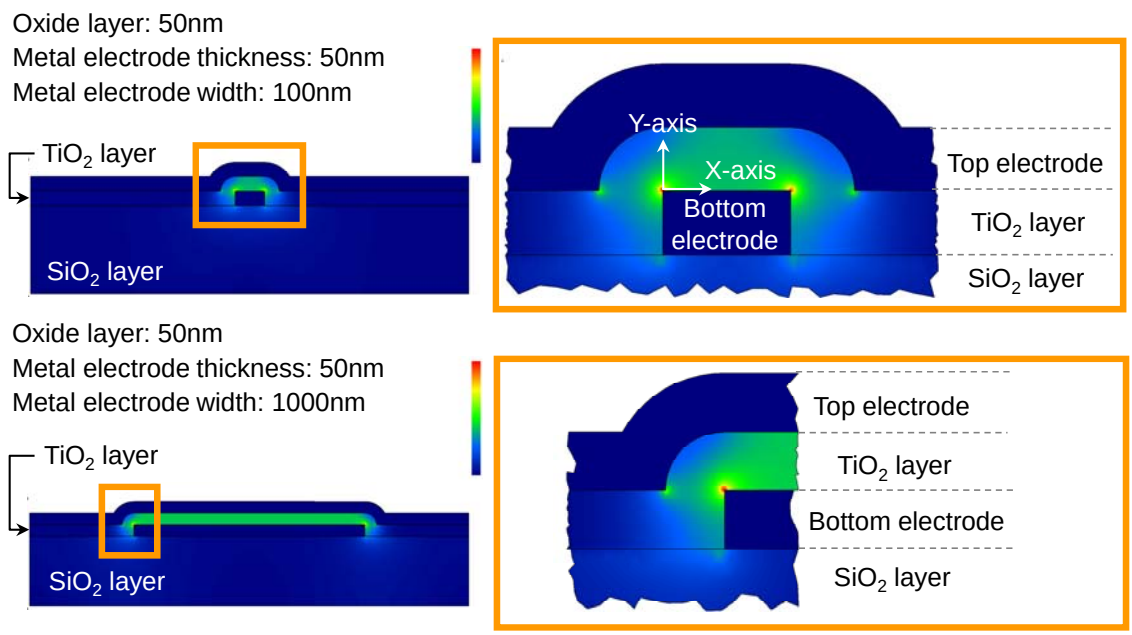

(b)

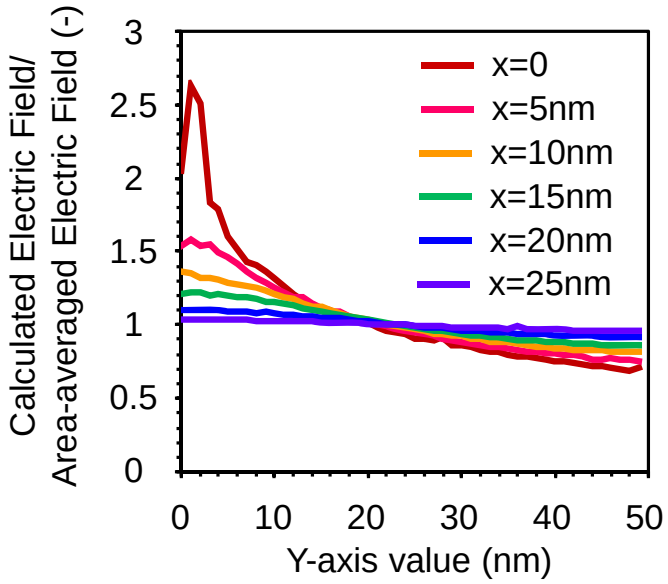

Figure S7 (a) Results of calculated spatial electric field distribution data. The comparison between two devices of different aspect ratios is shown. (b) Spatial distribution data of the ratio of calculated electric field to area-averaged electric field.

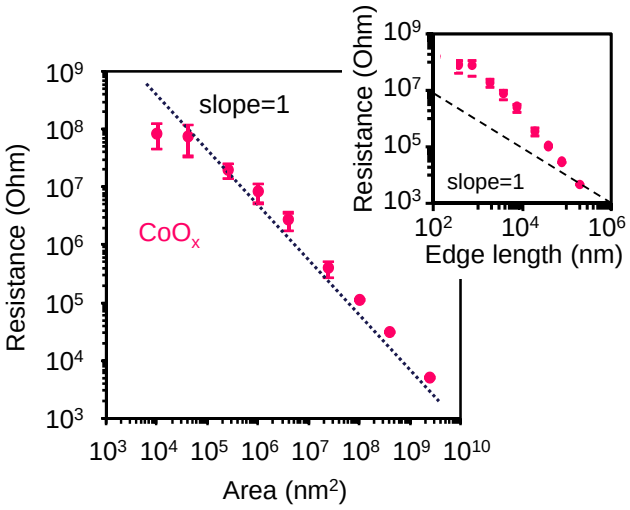

Figure S8 Relationship between cross-point area and resistance data. The data as a function of an edge length is also shown for comparison.

S4. Critical electric fields for bipolar switching behavior.

The presence of constant critical electric field in Fig.3 might correlate with the emergence of the bipolar switching. Among various models, a model based on an oxygen ion drift under an electric field has most successfully explained the features of bipolar switching. For low electric fields, an ionic drift velocity is proportional to an electric field, *i.e.* constant ion mobility. On the other hand, for high electric fields an ionic drift velocity exponentially increases with increasing an electric field. Strukov and Williams have proposed that such exponential ionic drift causes non-volatile bipolar switching behaviors by overcoming the effect of a thermal diffusion of ions.[7] Their model predicts that bipolar switching emerges above critical electric field E_0 where the exponential ionic drift occurs. They also estimated the E_0 value for titanium dioxides to be about 10^6 V/cm for 300 K using the formula $E_0=2k_BT/(qa)$, where k_B, T, q and a are the Boltzmann constant, temperature, charge of electron, and the jump distance of ions.

We have estimated E_0 values for our switching materials including NiO_x, CoO_x and TiO_{2-x}. In the estimations, the jump distance of ions is assumed to be a distance between nearest neighbouring oxygen sites for each material. The values of E_0 estimated from this formula and the observed experimental critical electric field for several materials are shown in Table S1. Considering that the model formula contains no arbitrary parameters at all, the observed agreement between the model estimations and the experimental values is excellent, highlighting that the model well captures the experimental trends. Thus the presence of critical threshold lines for bipolar switching can be rigorously interpreted in terms of an electric field required for an exponential ionic drift.

Table S1 Comparison between the averaged values of observed experimental critical electric field for bipolar switching and estimated values from the model based on an exponential ion drift

	CoO_x	TiO_{2-x}	NiO_x
Averaged experimental value of critical electric field (V/cm)	1.06 X10^6	0.89 X10^6	0.49 X10^6
Model estimated value (V/cm)	1.21 X10^6	1.10 X10^6	1.24 X10^6

S5. Weibull distribution data of electric fields required for unipolar switching and trends in the transition from bipolar to unipolar switching.

Figure S9 shows the distribution of the observed critical electric fields when varying the thickness, which conforms to a Weibull type distribution. Figure S10 shows the irreversible trend in the transition from bipolar to unipolar switching for CoO_x and NiO_x samples. When the forming currents were relatively low, the bipolar switching only occurred. When increasing the forming currents, the transition from bipolar to unipolar switching emerged via the forming process. Once the transition occurred, the stable unipolar switching behaviours were observed. However, when decreasing the forming current after such transition, the hysteresis loop in I-V data was strongly suppressed when compared with the original bipolar switching before the transition. These results highlight the strong irreversible trend of the transition for unipolar switching, demonstrating that the occurrence of unipolar switching is closely related to the irreversible nature of dielectric breakdown. [8-12]

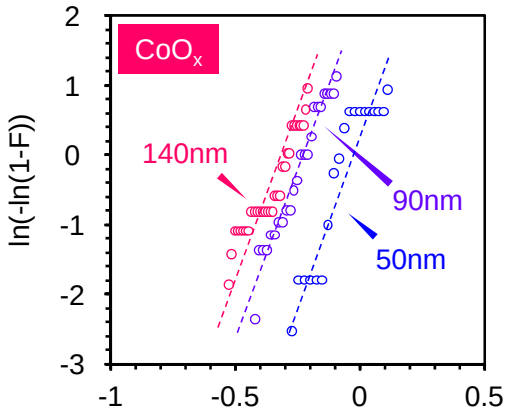

Figure S9 Weibull distribution data of electric fields required for an unipolar switching when varying the thickness of CoOx layer.

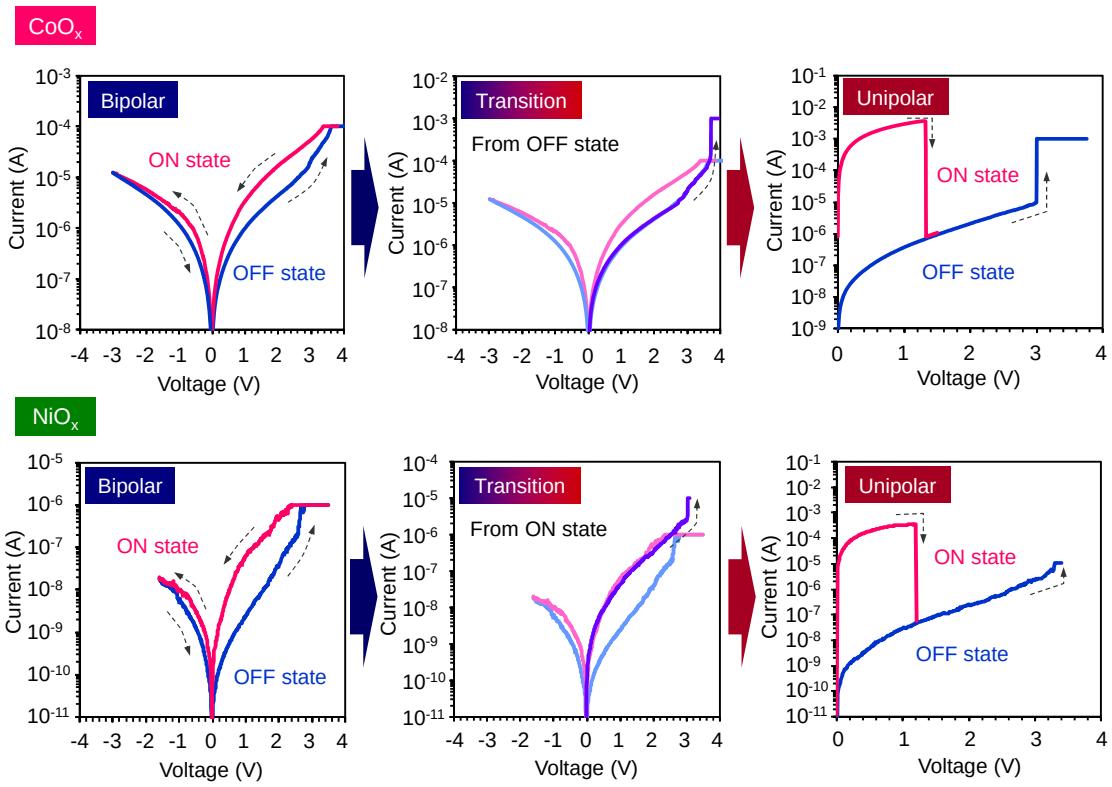

Figure S10 Irreversible trends in the transition from bipolar to unipolar switching in the case of CoO_x and NiO_x junctions. In the case of relatively low forming current, the bipolar switching behavior exhibited. Increasing the forming current resulted in the unipolar switching. Once the unipolar switching occurred, even decreasing the forming current did not show the same bipolar switching, demonstrating the Irreversible trends.

References

1. Nagashima, K., Yanagida, T., Tanaka, H., Seki, S., Saeki, A., Tagawa, S. & Kawai, T. Effect of the Heterointerface on Transport Properties of in Situ Formed MgO/Titanate Heterostructured Nanowires. *J. Am. Chem. Soc.* **130**, 5378-5382 (2008).
2. Oka, K., Yanagida, T., Nagashima, K., Tanaka, H., Seki, S., Honsho, Y., Ishimaru, M., Hirata, A. & Kawai, T. Specific surface effect on transport properties of NiO/MgO heterostructured nanowires. *Appl. Phys. Lett.* **95**, 133110 (2009).
3. Nagashima, K., Yanagida, T., Oka, K., Taniguchi, M., Kawai, T., Kim, J.-S. & Park, B.-H. Resistive Switching Multistate Nonvolatile Memory Effects in a Single Cobalt Oxide Nanowire. *Nano Lett.* **10**, 1359-1363 (2010).
4. Nagashima, K., Yanagida, T., Klamchuen, A., Kanai, M., Oka, K., Seki, S. & Kawai, T. Interfacial effect on metal/oxide nanowire junctions. *Appl. Phys. Lett.* **96**, 073110 (2010).
5. Oka, K., Yanagida, T., Nagashima, K., Kawai, T., Kim, J.-S. & Park, B.-H. Resistive-Switching Memory Effects of NiO Nanowire/Metal Junctions. *J. Am. Chem. Soc.* **132**, 6634-6635 (2010).
6. Oka, K., Yanagida, T., Nagashima, K., Tanaka, H. & Kawai, T. Nonvolatile Bipolar Resistive Memory Switching in Single Crystalline NiO Heterostructured Nanowires. *J. Am. Chem. Soc.* **131**, 3434-3435 (2009).
7. Strukov, D. B. & Williams, R. S. Exponential ionic drift: fast switching and low volatility of thin-film memristors. *Appl. Phys. A* **94**, 515-519 (2009).
8. Lombardo, S. et al. Dielectric breakdown mechanisms in gate oxides. *J. Appl. Phys.* **98**, 121301 (2005).

9. Satoh, T. & Tanaka, R. Area effect and distance effect of transformer oil insulation, *Aichi Denki Gihou*, **28**, 12-17 (2007).
10. Hidaka, K. Koudenatsu Kougaku. (Suuri Kougakusya, Tokyo, 2009).
11. O'Dwyer, J. J. Theory of Dielectric Breakdown in Solid. *J. Electrochem. Soc.* **116**, 239-242 (1969).
12. Lee, J. S. & Kahng, B. Scaling behaviours of the voltage distribution in dielectric breakdown networks. *Phys. Rev. E* **83**, 052103 (2011).